Supporting information

S1. Records used in this study

*Table S1: Radionuclide records used in the study and their characteristics. *The ^{14}C production rate in the carbon cycle model is 1 (idealized units) for present day ($\Delta^{14}C$=0 ‰). The global average ^{14}C production is approximately 2 atoms cm^{-2} s^{-1} (1).*

Record	Nuclide	Source	Time span (year BP)	Temporal resolution (years)	Ref.	Mean value to normalize data in Fig. 2 (10^4 atoms/g)
INTCAL09	^{14}C	Tree-rings	9400 to 150	5-10	(2)	1*
EDML	^{10}Be	Ice Antarctica	9400 to 1200	4-5	**New**	4.1
GRIP	^{10}Be	Ice Greenland	9400 to 300	4-5	(3), (4)	1.5
Dye-3	^{10}Be	Ice Greenland	526 to -35	1	(5)	1.1
Milcent	^{10}Be	Ice Greenland	769 to 148	3-4	(6)	1.1
NorthGRIP	^{10}Be	Ice Greenland	561 to -44	1	(7)	1.8
South Pole	^{10}Be	Ice Antarctica	1107 to -32	~8	(8)	3.8
Dome Fuji	^{10}Be	Ice Antarctica	1255 to 75	10	(9)	9.4

S2. Description of the ^{10}Be EDML record

The EDML ice core was drilled within the framework of the European Project for Ice Coring in Antarctica (EPICA) located at Dronning Maud Land (DML) (75 0.10' S, 0 4.07' E, 2882 m), Antarctica(10). The ^{10}Be record used herein covers the period from 1,193 BP to 9,400 BP (corresponding to a depth range from 113 m to 585 m). The processing of the EDML ice core took place at Alfred-Wegener Institute / Bremerhaven in a joint action by the institutes involved in EPICA.

The chemical preparation of the ^{10}Be samples was done at Eawag in Dübendorf/Switzerland. The ice was cut into samples of 25 cm length (about 100g of ice per sample), corresponding to an average sample temporal resolution of about 4.5 years throughout the Holocene. Then the ice was melted in a microwave oven, mixed with 0.125 mg of ^{9}Be carrier and passed through a cation ion exchange resin. We did not use any filters. The chemical preparation was done in the same way as for the ^{10}Be samples from the GRIP ice core (see (3), (4)). The ^{10}Be samples were measured at the accelerator mass spectrometer (AMS) facility of ETH Zurich, Switzerland. The typical AMS counting uncertainty of the ice core samples is about 5 %. The results were normalized to the ETH standard S555N(11).

We use the time scale called EDML1(12). ^{10}Be fluxes are obtained by multiplying the ^{10}Be concentrations with the corresponding accumulation rates from Ref. (12).

S3. Remarks to ^{10}Be measurements

The different ^{10}Be records, which were used in this study, have been normalized to different AMS standards. Because we are interested in the relative variations only, we normalized the records to their respective mean values.

S4. ^{10}Be half-life correction

We applied a decay correction to the ^{10}Be records, using a half-life of (1.387+-0.012) million years ((13, 14)).

S5. ^{14}C production rate

We applied a box-diffusion carbon cycle model (15) to calculate the production rate p14C from the atmospheric ^{14}C concentrations as measured in tree rings (2). Thereby we assumed that the carbon cycle has been stable throughout the Holocene.

S6. Determination of common production rate (cosmic ray intensity) with principal component analysis (PCA)

The individual radionuclide records used here cover different time periods. In order to remove the system effects (see article) from the records we applied PCA instead of using mean values. A prerequisite of PCA is that the input data have the same sample resolution and cover the same time interval. First we divided each record into a series of consecutive 22-year intervals with the interval centers being the same in all records. The data points in each interval were averaged and this average was assigned to the central age. The principal components (PCs) were built from eight blocks (Table S2) of records with each block containing between 2 to 6 individual radionuclide records.

Table S2: Blocks of records used in PCA and for determining the common production rate (cosmic ray intensity). Time series and resulting common cosmic ray intensity are shown for the individual blocks 1-8 in Figures S1-S8. Year BP=before present (1950AD). 1.PC=First principal component.

Block number	Records used (number of records)	Time interval in PCA (year BP)	Used time interval (year BP)	Total variance described by 1.PC	Normalization period (year BP)
1	Dye-3, NorthGRIP, South Pole (3)	534 to -38	72 to -38	76%	6 to -38 (1944-1988 AD)
2	Dye-3, NorthGRIP, South Pole, Dome Fuji (4)	534 to 72	138 to 72	72%	544 to 72
3	Dye-3, NorthGRIP, South Pole, Dome Fuji, INTCAL09-p14c, Milcent (6)	534 to 149	534 to 138	67%	544 to 138
4	South Pole, Dome Fuji, INTCAL09-p14c, Milcent, GRIP (5)	776 to 292	776 to 534	72%	544 to 292
5	GRIP, Dome Fuji, South Pole, INTCAL09-p14c (4)	1128 to 292	1128 to 776	82%	765 to 292
6	GRIP, Dome Fuji, INTCAL09-p14c (3)	1260 to 292	1194 to 1128	88%	1128 to 292
7	GRIP, p14C (2)	9400 to 292	Used for normalization only (see note below)	77%	1260 to 292
8	EDML, GRIP, INTCAL09-p14c (3)	9400 to 1194	9400 to 1194	69%	2206 to 1194

Before applying PCA all records were standardized by subtracting the mean and dividing by the standard deviation of the individual records. PCA gives as many principal components as input records are used. We consider only the first principal component, which describes most of the total variance in all records shown as percentages of the total variance in Table S2. Because the records used as input data fort PCA were standardized the PCs are also in standardized units. To obtain

physical units, the first PC was first multiplied with the standard deviation of the individual records and second the mean of the individual records was added. Then all records were divided by their mean value. These records in each block show the common signal of those records in units relative to their individual mean. We calculated the mean value of these records which is the "mean common signal" of the corresponding block.

The mean common signals are then normalized in such a way that the mean signal is equal to the signal of the previous block in their overlapping interval (Table S2, Figures S1-S8). This was done by dividing the block by its mean in the overlapping interval with the previous block and by multiplying the block with the mean of the previous block in the overlapping interval. The blocks are based on different datasets and cover different time periods and therefore the variance is not equal in the individual blocks. This is the reason that we only adjust the mean of a block with the former block but not the variance. The variances are compared in Table S3. The normalization periods for consecutive blocks are shown in the last column of Table S2. Block 1 has been normalized in such a way that the average signal in the period 1944-1988 is 1. The normalization periods for blocks 2-7 are the entire overlapping interval with the former block. Block 8 was normalized with Block 7 over 1000 years in the youngest part of the overlapping period. Finally mean curves are calculated for each block. The mean curves of the eight blocks are combined to represent the common production signal variation (cosmic ray intensity).

Block number	Records used (number of records)	Variance in overlapping interval (normalized units) (former block, this block)	Ratio former block/this block
1	Dye-3, NorthGRIP, South Pole (3)		
2	Dye-3, NorthGRIP, South Pole, Dome Fuji (4)	0.17, 0.175	0.97
3	Dye-3, NorthGRIP, South Pole, Dome Fuji, INTCAL09-p14c, Milcent (6)	0.18, 0.17	1.02
4	South Pole, Dome Fuji, INTCAL09-p14c, Milcent, GRIP (5)	0.15, 0.14	1.1
5	GRIP, Dome Fuji, South Pole, INTCAL09-p14c (4)	0.15, 0.16	0.89
6	GRIP, Dome Fuji, INTCAL09-p14c (3)	0.16, 0.16	0.97
7	GRIP, p14C (2)	0.16, 0.16	1.0
8	EDML, GRIP, INTCAL09-p14c (3)	0.11, 0.09	1.18

Table S3: Comparison of variances in the overlapping intervals of the block and the former block.

Note, that block 6 overlaps with block 8, but the overlap interval consists of only three data points from the years 1260-1194BP which is not long enough for an accurate normalization. Hence we did not use block 6 to normalize block 8. We introduced block 7 based only on GRIP ^{10}Be data and p^{14}C. This block was normalized with block 6, and then used to normalize block 8. Block 7 and

block 8 cover the same time span back to 9400 BP, but because block 8 considers also EDML ^{10}Be, it is a more robust record of cosmic ray intensity over the entire period.

The following figures illustrate how the records were normalized and combined to obtain the 9400-year record. Every figure has three panels. In the top panel the raw 22-year averages of the various radionuclide records used for the time interval of the block are shown. The middle panel shows the common average first principal component (1.PC) using all records and leaving out one record (jackknife method) together with the percentage described by the 1.PC (eigenvalue of the 1.PC). The bottom panel shows how the corresponding block agrees with the previous block within the overlapping interval to build the composite. The redish intervals mark the periods used to normalize the two corresponding blocks.

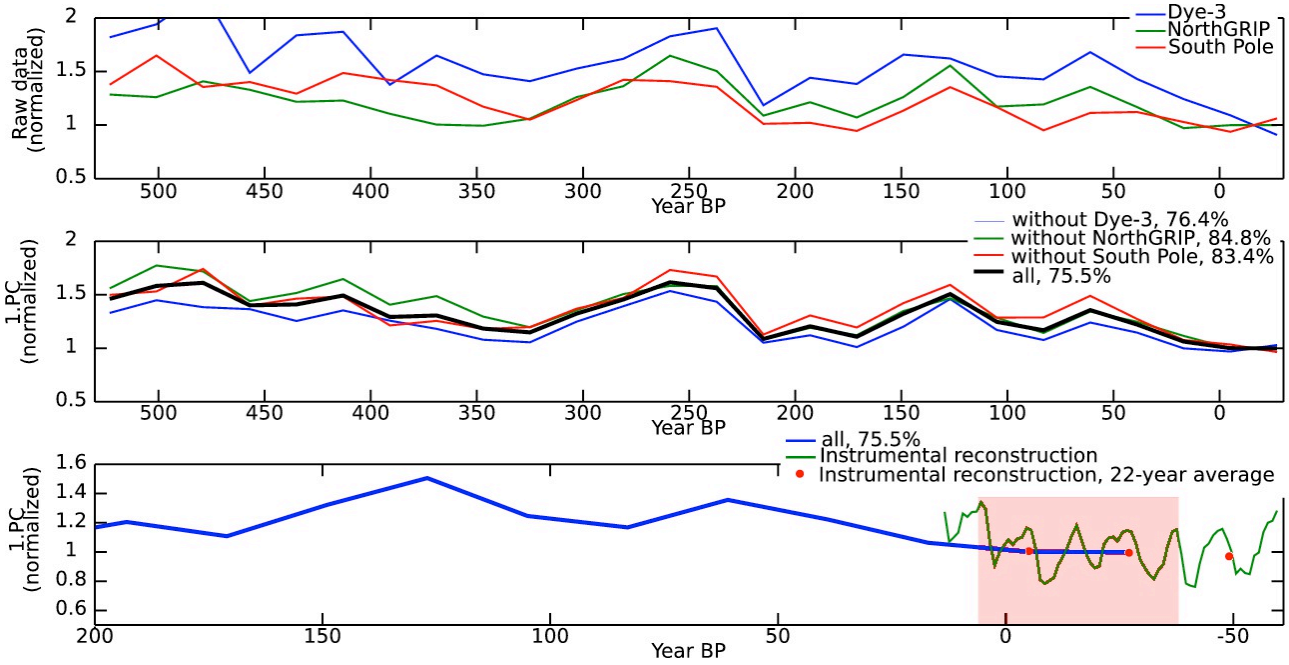

Figure S1 Normalization of block 1. The redish interval is used as normalization period (for details see section 9 and Figure S11). Instrumental reconstruction based on neutron monitor and ionization chamber data (see section S9 for details).

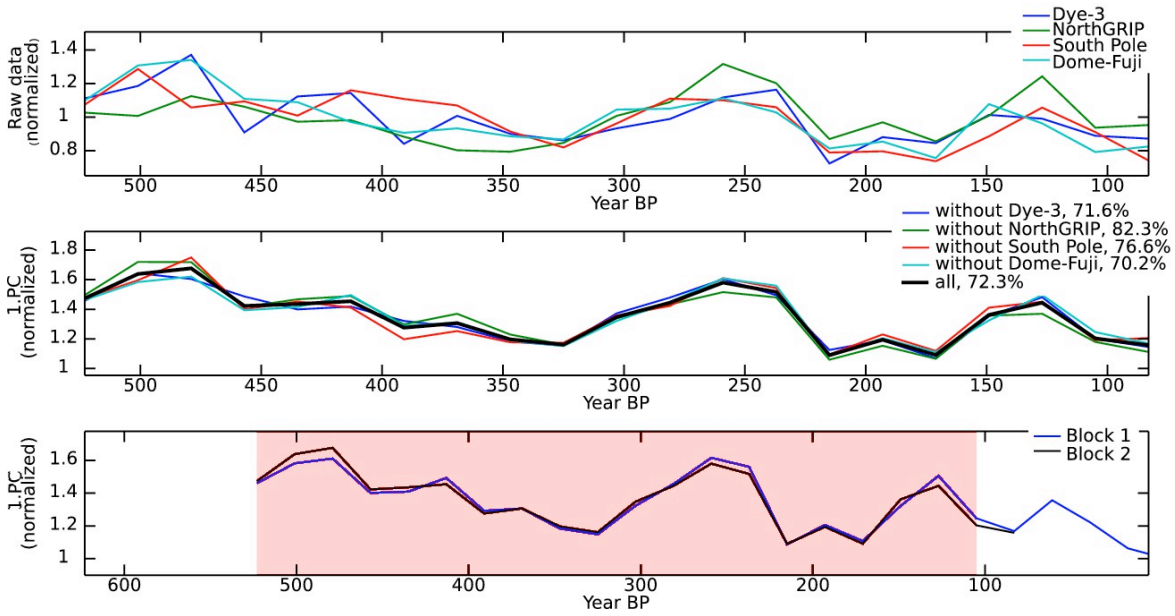

Figure S2 Normalization of block 2. The redish interval is used as normalization period.

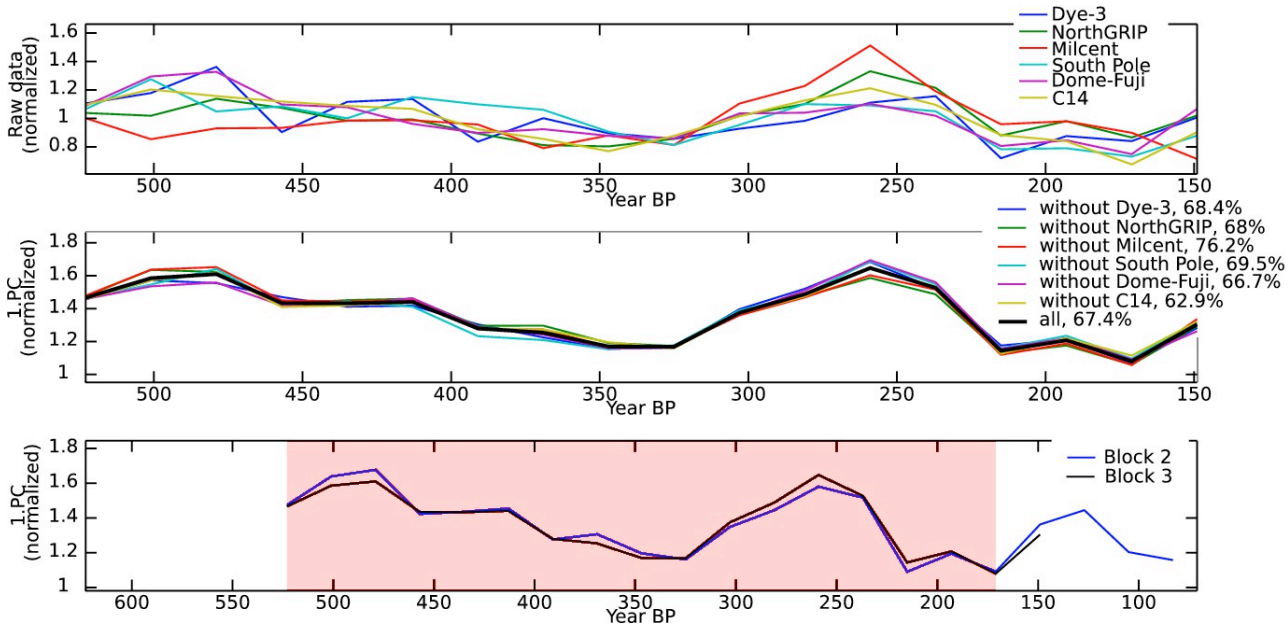

Figure S3 Normalization of block 3. The redish interval is used as normalization period.

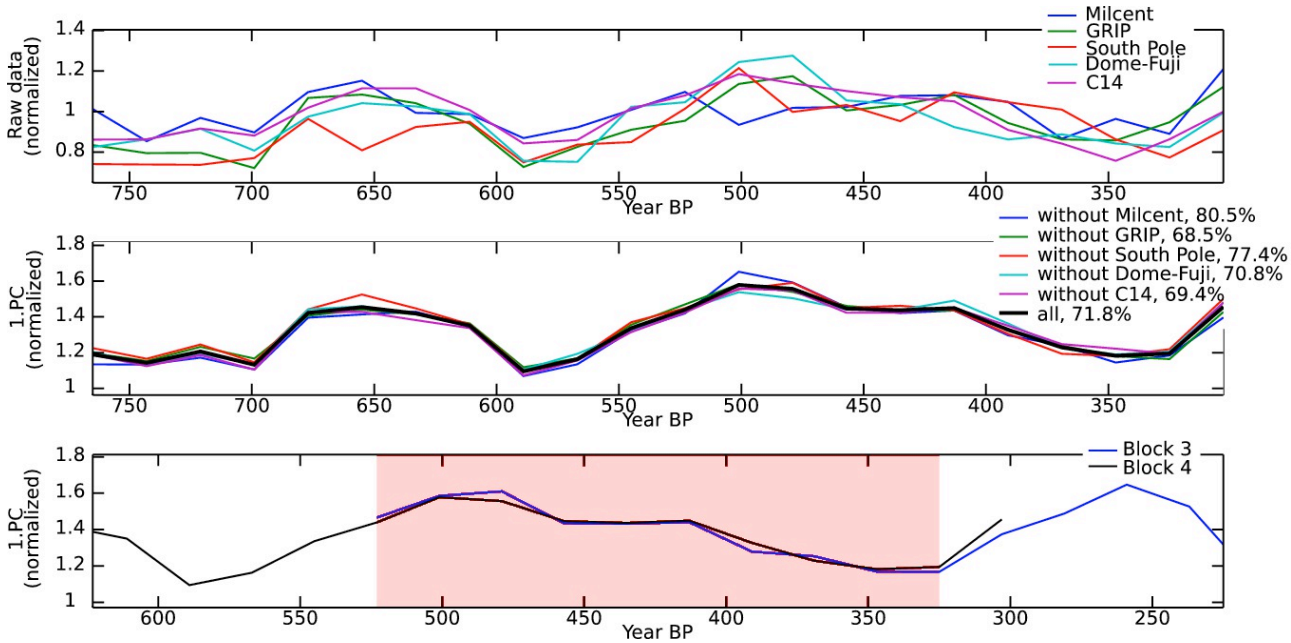

Figure S4 Normalization of block 4. The redish interval is used as normalization period.

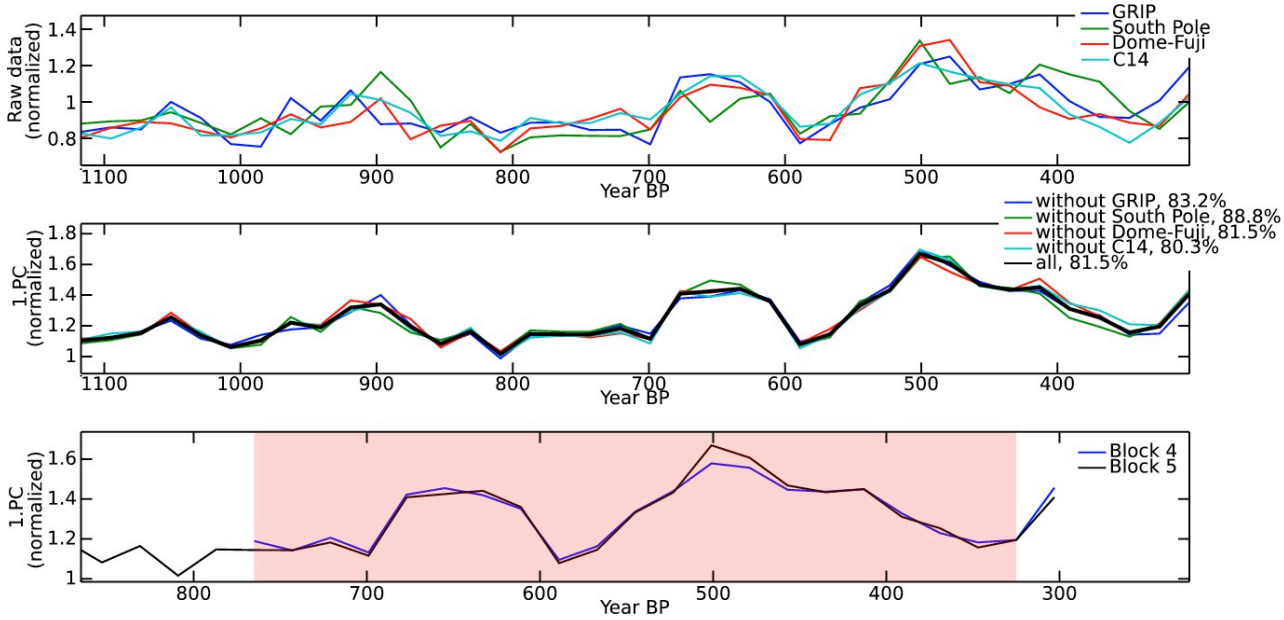

Figure S5 Normalization of block 5. The redish interval is used as normalization period.

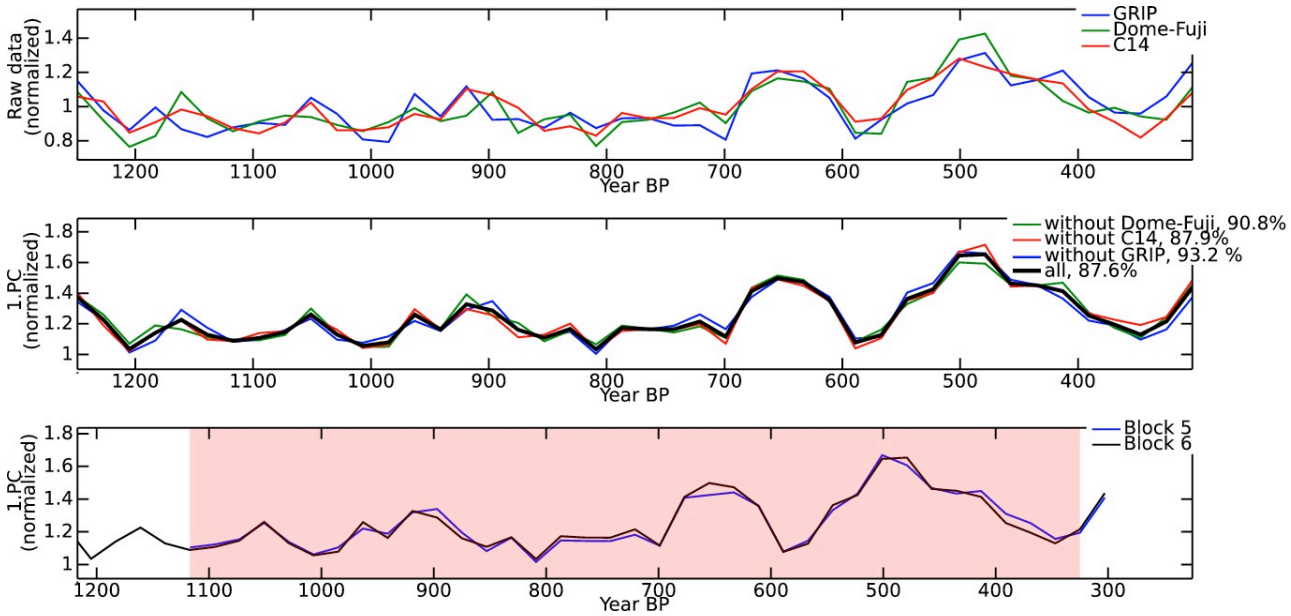

Figure S6 Normalization of block 6. The redish interval is used as normalization period.

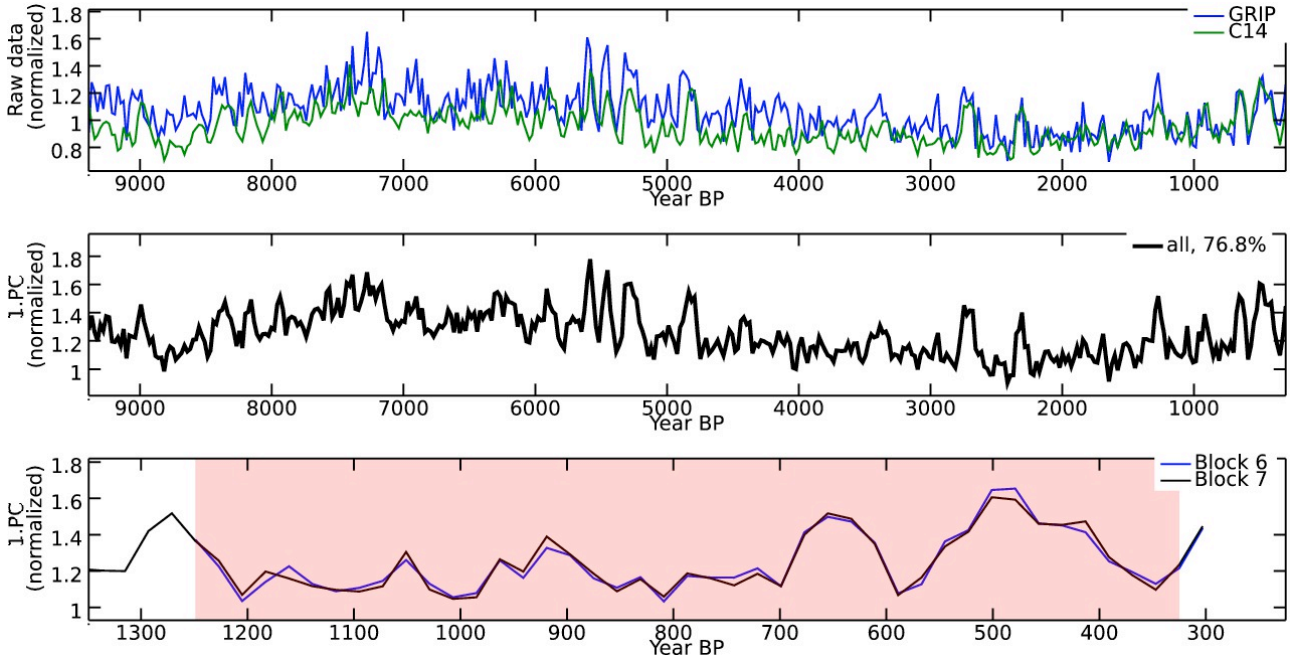

Figure S7 Normalization of block 7. The redish interval is used as normalization period. Note, that in this block jackknife could not be applied because of only two records (GRIP and 14C).

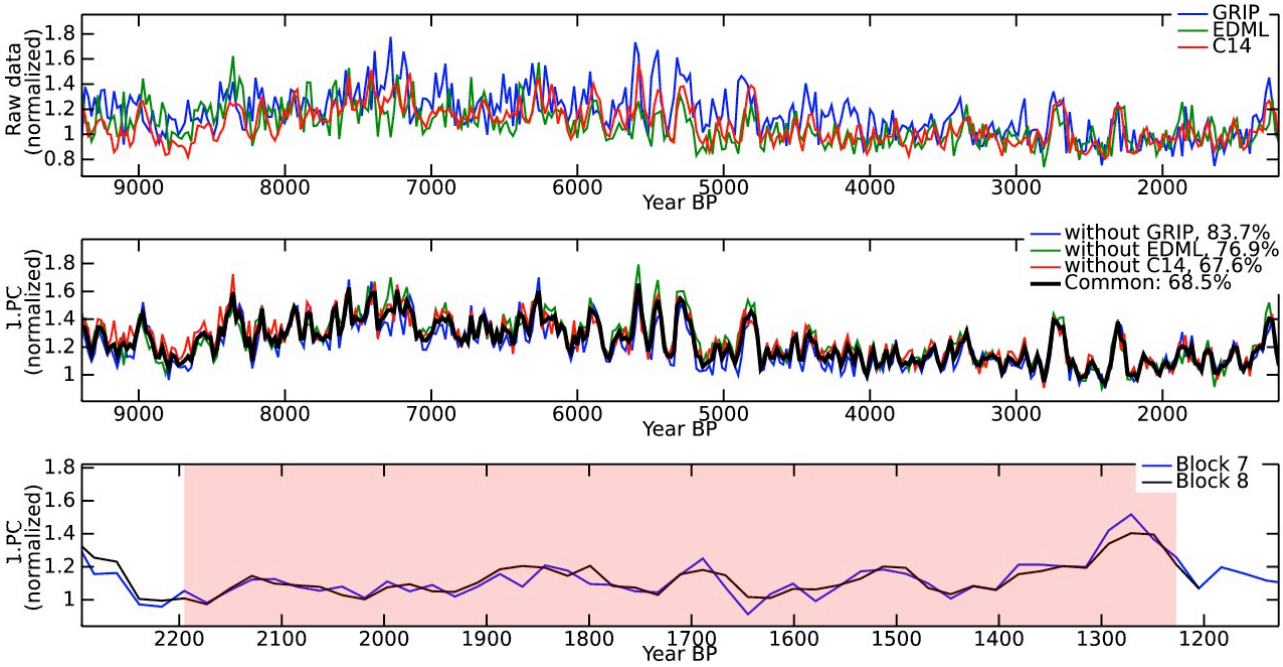

Figure S8 Normalization of block 8. The redish interval is used as normalization period.

S7. Comparison of cosmic ray intensity based on concentrations and fluxes

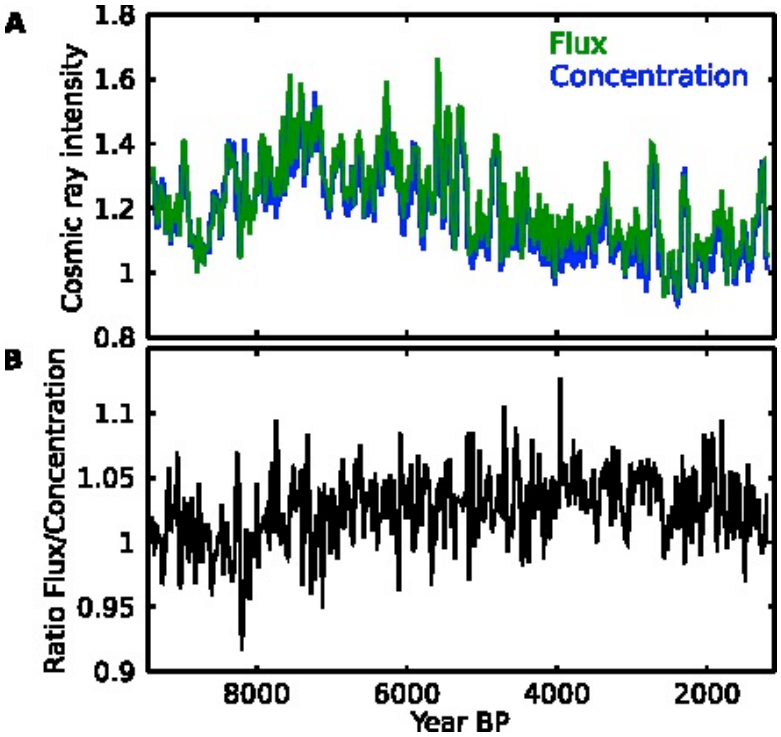

Figure S9: Relative cosmic ray intensity based on the principal component analysis of the radionuclide records averaged over 22 years. Time is given in year BP. **A** *The blue curve is based on ^{10}Be concentrations (EDML and GRIP) and p14C; the green curve is based on ^{10}Be fluxes (EDML and GRIP) and p14C.* **B** *Ratio of flux and concentration based reconstructions of the relative cosmic ray intensity from panel A. The two reconstructions of cosmic ray intensity differ by less than 5% on average.*

S8. Determination of the uncertainty of the cosmic ray record

To determine the robustness of the common production signal, we used the jackknife method, which means we applied PCA by leaving out individual radionuclide records. In every block PCA was done as often as radionuclide records are considered. By doing so every radionuclide record has been left out in one PCA calculation. Therewith, lower and upper curves of the common production signal could be determined. The maximal difference between the lower and upper curves and the production signal, when all radionuclide records are considered, is the herein called maximal jackknife uncertainty. This uncertainty is shown in Figure S10 as a function of time. In addition the standard deviation of the "raw" radionuclide records is shown. Figure S11 shows the corresponding distributions. It can be seen that already the "raw" radionuclide records do differ on average by less than 10 %. The jackknife uncertainty is on average 5 %. As a conservative estimate we use the standard deviation of the "raw" radionuclide records as uncertainty of the final common production rate record (as shown as cosmic ray intensity in Figure 3 B, C, D).

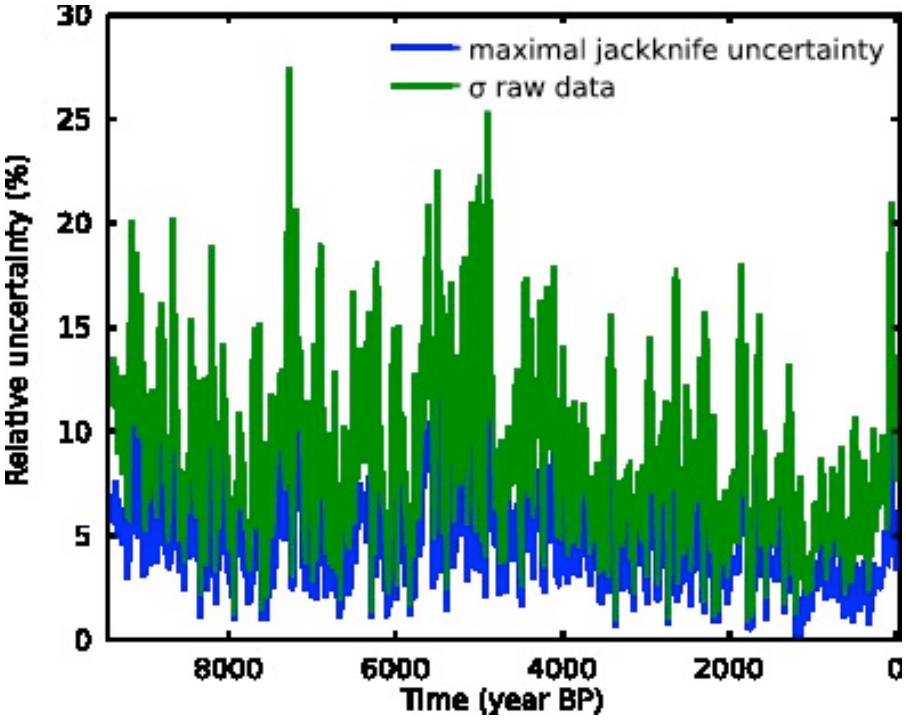

Figure S10: Comparison of uncertainty in time: jackknife method and standard deviation of "raw" radionuclide records. Time is given in year BP.

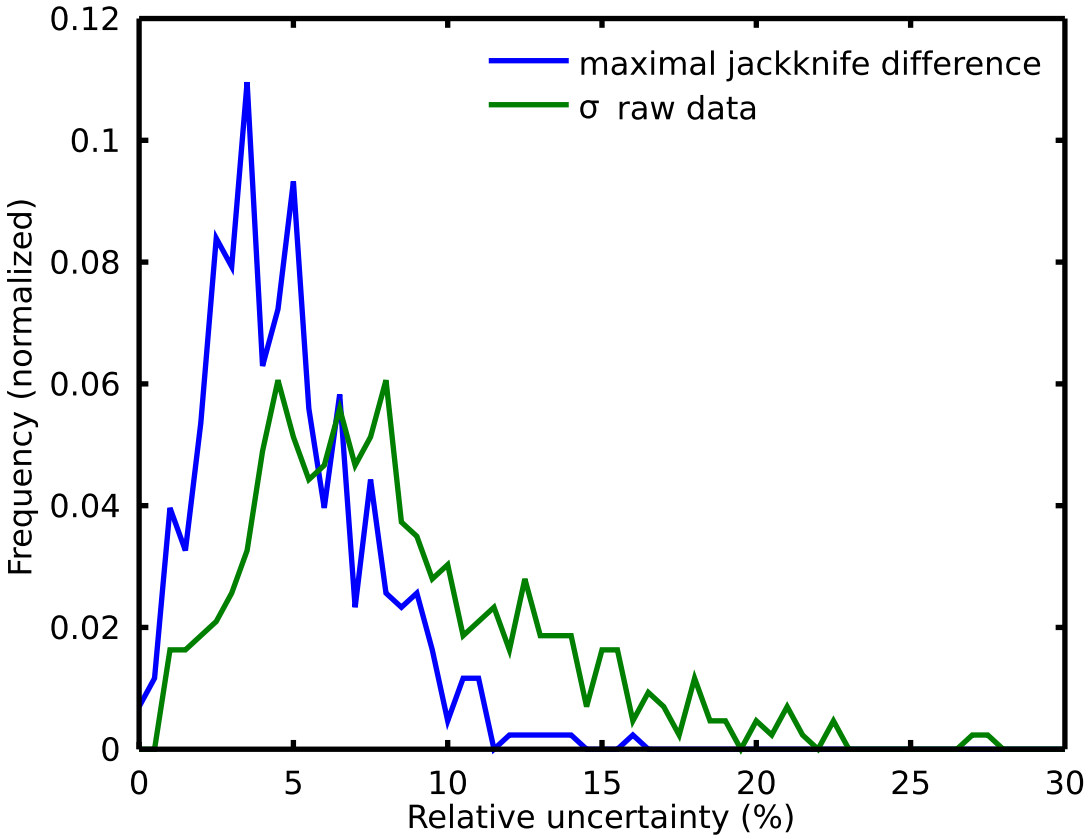

Figure S11: Comparison of uncertainty distribution: jackknife method and standard deviation of "raw" radionuclide records. Distributions are normalized by the integral over all uncertainty bins.

S9. Calculation of ^{10}Be production for the period 1937-2010 from neutron monitor and ionization chamber data

To compare the 9400-year long record of cosmic ray intensity with the most recent years, neutron monitor and ionization chamber data are used to calculate cosmic ray intensity. These data allow determining the solar modulation potential Φ (16). The solar modulation potential Φ is a parameter describing the cosmic ray intensity modulation outside the Earth's magnetic field. The Φ data of (16) are available as monthly means. We averaged the monthly means to 22-year averages equal to the radionuclide records of this study. This Φ record is based on another interstellar spectrum than the production calculation by (1) which has been corrected using the approach described in (17). The 22-year averages of the Φ record were used together with the radionuclide production calculations by (1) to calculate the ^{10}Be production during the instrumental (neutron monitor and ionization chamber) era. Figure S12 compares the ^{10}Be production calculated from the three 22-year average data points of Φ with the common production rate from the radionuclide records. The ^{10}Be production rate calculated for the annual averages of Φ is also shown. Both the radionuclide based and the instrumental based records are normalized for the same period of 1944-1988, and can therefore be directly compared with each other. The reconstructed annual ^{10}Be production rate varies inversely proportional to the 11-year solar cycle with a relative change between solar minima and maximum from 0.8 to 1.2. Multi-decadal variability is practically absent in the recent decades, i.e. the long-term variability of the ^{10}Be production (cosmic ray intensity) has been very low during this period compared with the past 200 years as shown in Fig. S12.

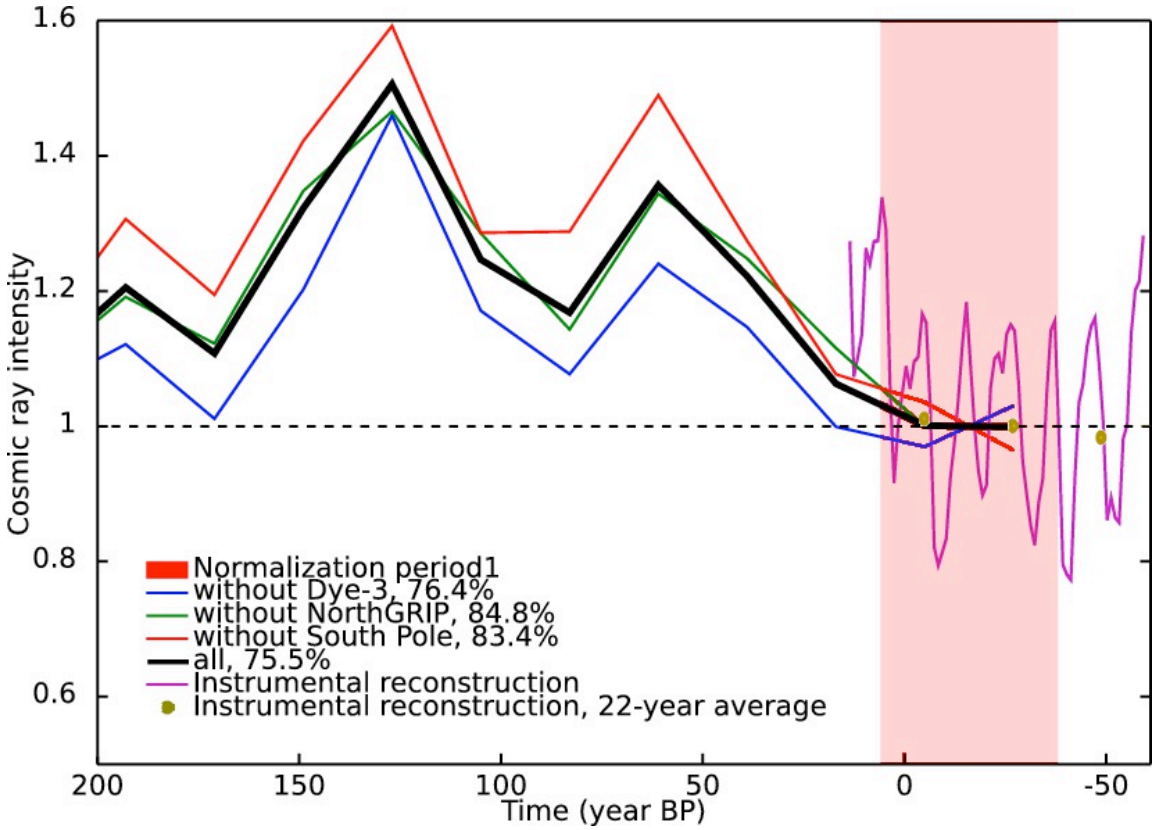

Figure S12: Comparison of cosmic ray intensity obtained with cosmogenic radionuclides and with instrumental data (neutron monitors and ionization chambers). Time is given in year BP. Data are normalized to the period of 1944-1988AD (6 to (-38) BP).

S10. Reconstruction of solar activity (total solar irradiance) from the cosmic ray intensity record

We reconstructed the solar activity (total solar irradiance) from the cosmic ray record using the methods as described in refs.(17-20).

First, we reconstructed the solar modulation potential (21), which is a measure of the solar modulation of the cosmic ray particles by removing the effect of the geomagnetic field (1) based on paleomagnetic data reconstructed in ref. (22). The details of this procedure are described in references (1, 17, 20). The Φ reconstruction is shown in Fig. S13. During some very deep solar minima negative values of Φ occur, which is impossible from the physical point of view. As discussed in ref. (23) different explanations exist for the occurrence of negative values such as the uncertainties in radionuclide records, in radionuclide production calculations, in geomagnetic field strength reconstructions, and in the estimation of the local interstellar spectrum.

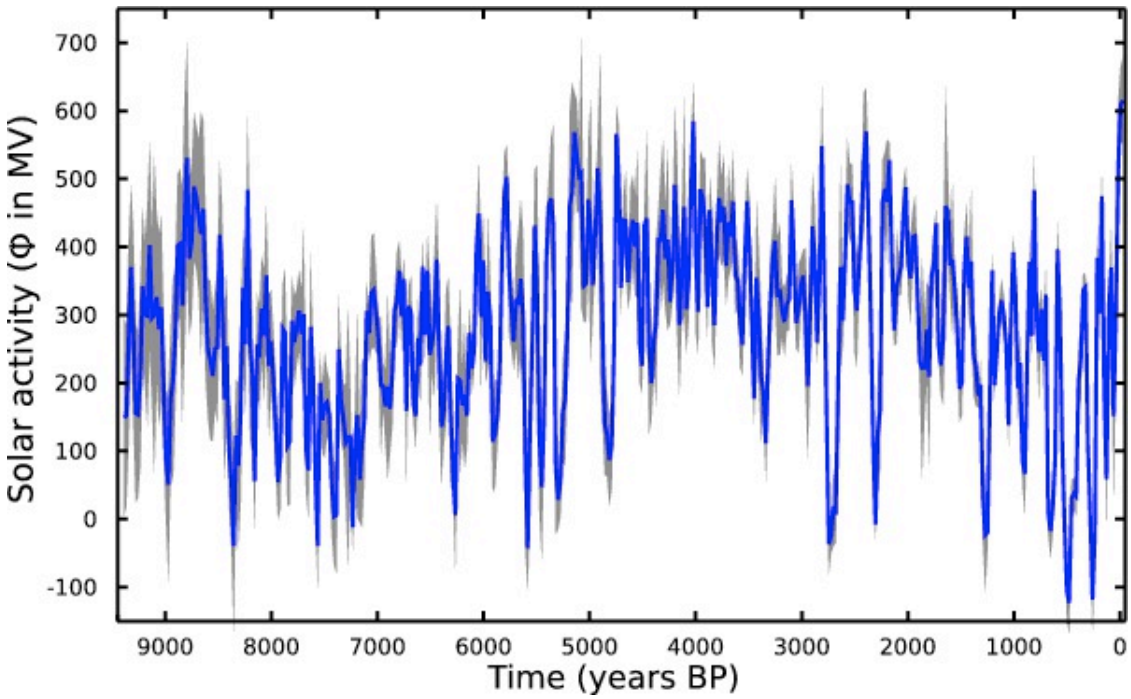

Figure S13 Solar modulation potential Φ reconstructed from the common cosmic ray intensity record. The paleomagnetic field has been removed (22). Φ is calculated with the local interstellar spectrum from ref. (24). Uncertainty is one standard deviation obtained from 1000 Monte Carlo simulations considering uncertainties in cosmic ray record and geomagnetic field strength. Time is given in year BP. Note that the variation on the millennial time-scale of Φ depends on the geomagnetic field. If another geomagnetic field reconstruction like for example ref (25) were used Φ would show another (long-term) trend on millennial time scales.

Then, the strength of the interplanetary magnetic field is calculated using its physical relationship with solar modulation potential Φ as given in refereces (18, 19). Figure S14 shows the reconstructed interplanetary magnetic field for the period 1880 to the present day. Independent reconstructions of the interplanetary magnetic field based on geomagnetic indices (26) are also plotted. As can be seen our reconstruction agrees reasonably well with the ones based on geomagnetic indices.

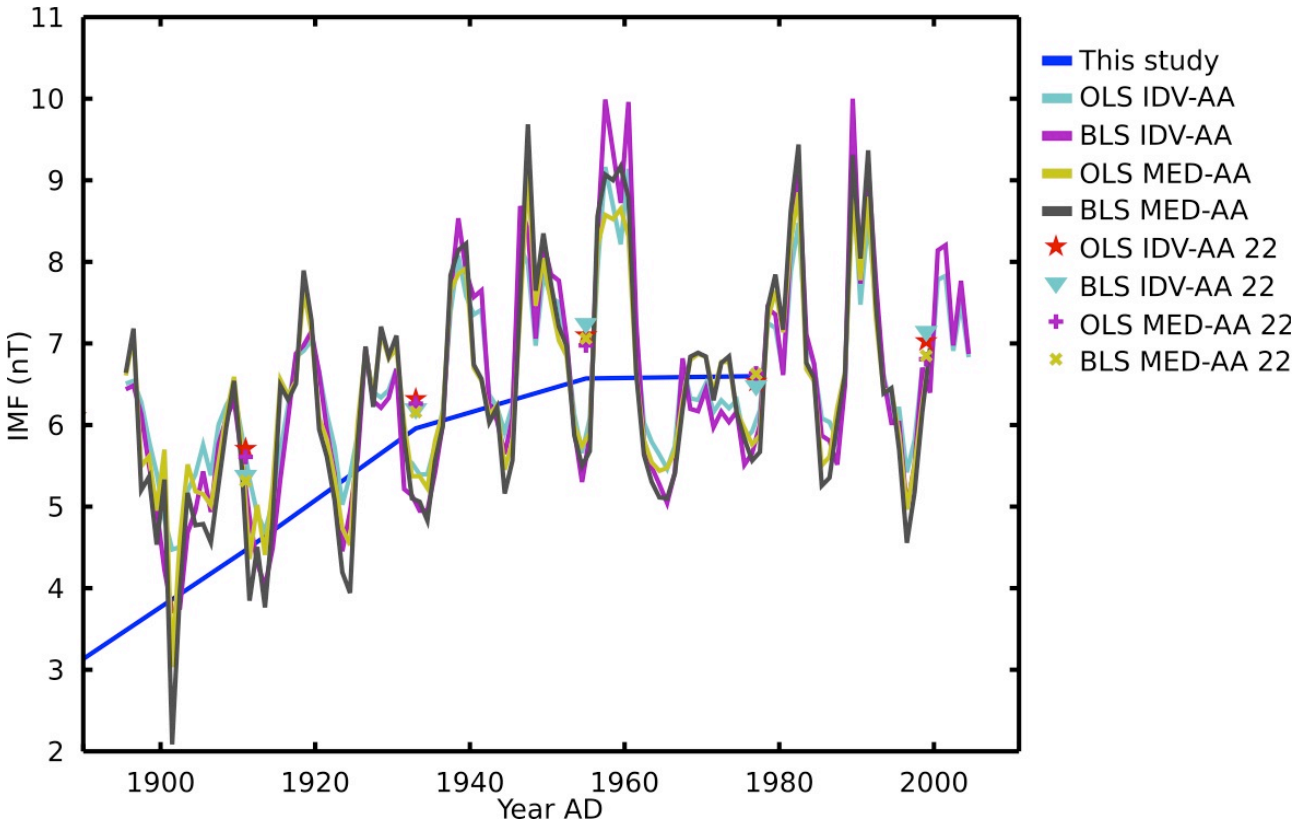

Figure S14 Comparison of interplanetary magnetic field reconstructed from Φ using their physical relationship as given in references (18, 19) (blue curve) with geomagnetic indices based reconstructions (26). The stars, diamonds, pluses, and crosses are 22-year averages of the geomagnetic indices-based reconstructions (same color code as the yearly records).

Third, total solar irradiance is calculated using its observed relationship with the strength of the interplanetary magnetic field (27). The time series of total solar irradiance over the Holocene is shown in Fig. S15. The data set will be available online at the NOAA paleo server (http://www.ncdc.noaa.gov/paleo/forcing.html).

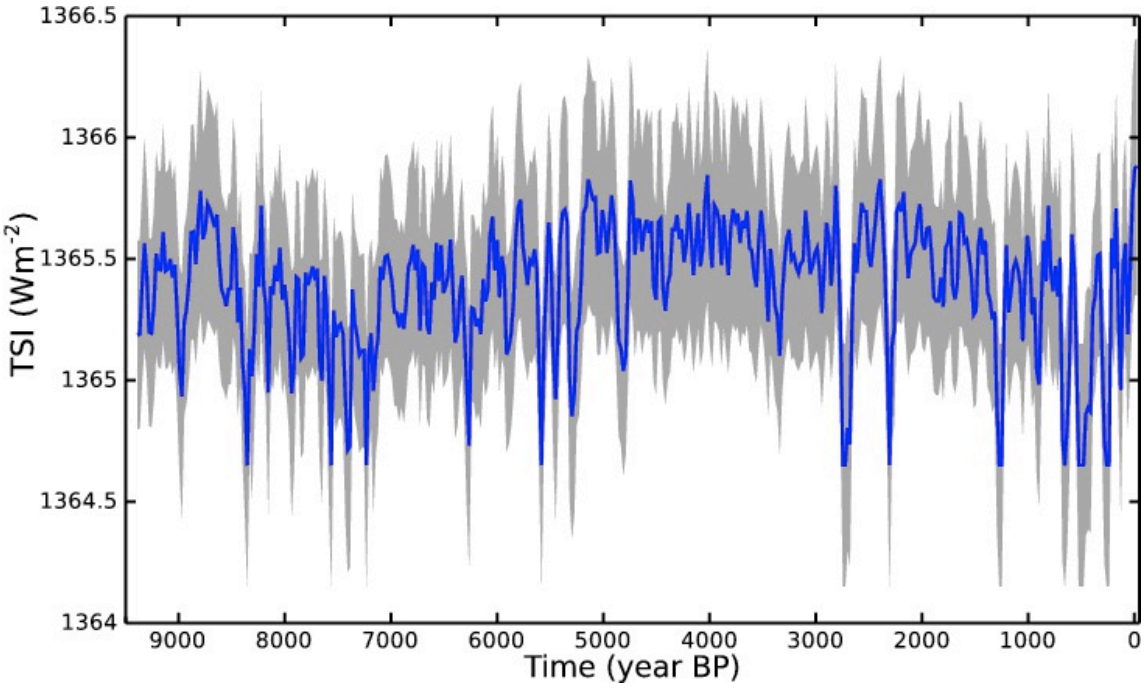

Figure S15 Total solar irradiance calculated using the method given in ref. (19). Time is given in

year BP. Gray shaded uncertainty is one standard deviation obtained from uncertainties in Φ (see Fig. S12), in the relationship of Φ with the interplanetary magnetic field (18, 19), and in the relationship between interplanetary magnetic field and total solar irradiance (27).

S11. Power spectra of total solar irradiance (Figure S16) and $\delta^{18}O$ from Dongge cave

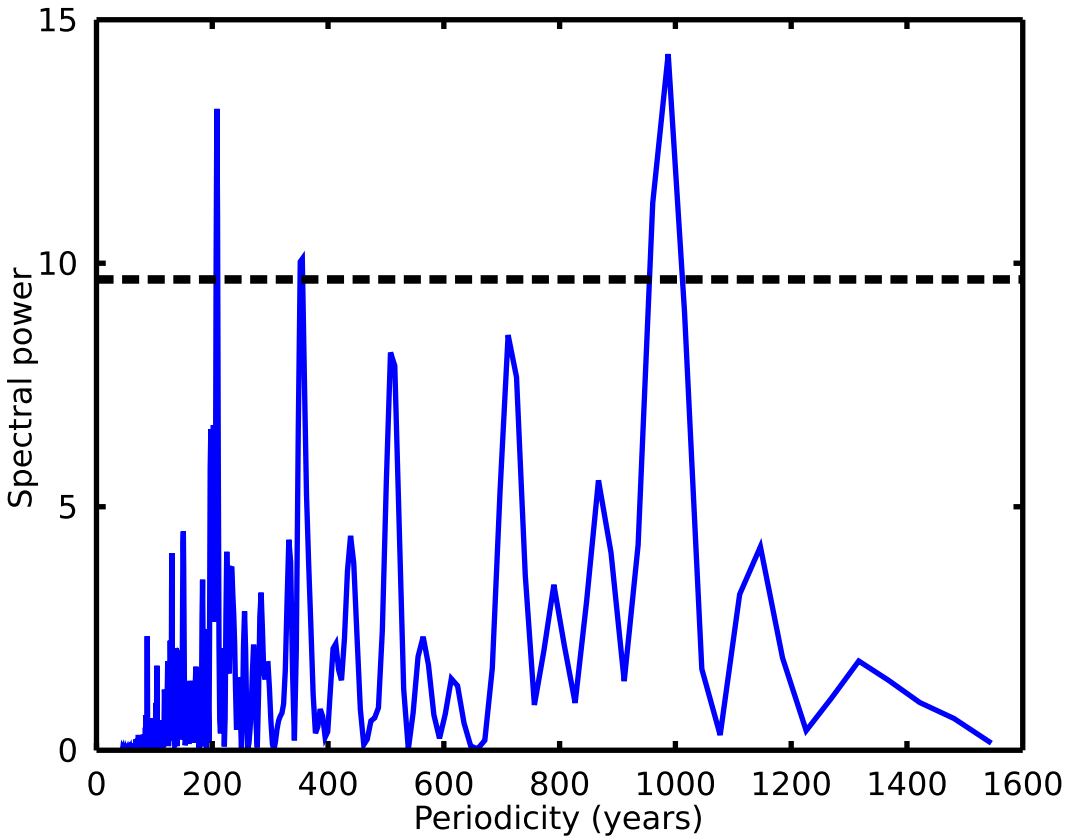

Figure S16 Lomb normalized periodogram (spectral power as a function of periodicity) of total solar irradiance. The horizontal dotted line marks the 95% significance level. Prominent periodicities are the de Vries cycle at ~210 years and the Eddy cycle at ~1000 years (28). These periodicities are used in Fig. 4 of the paper to detect the solar fingerprint in an Asian climate record ($\delta^{18}O$ from Dongge cave, China, (29)). See Figure S17 for periodogram of the climate record.

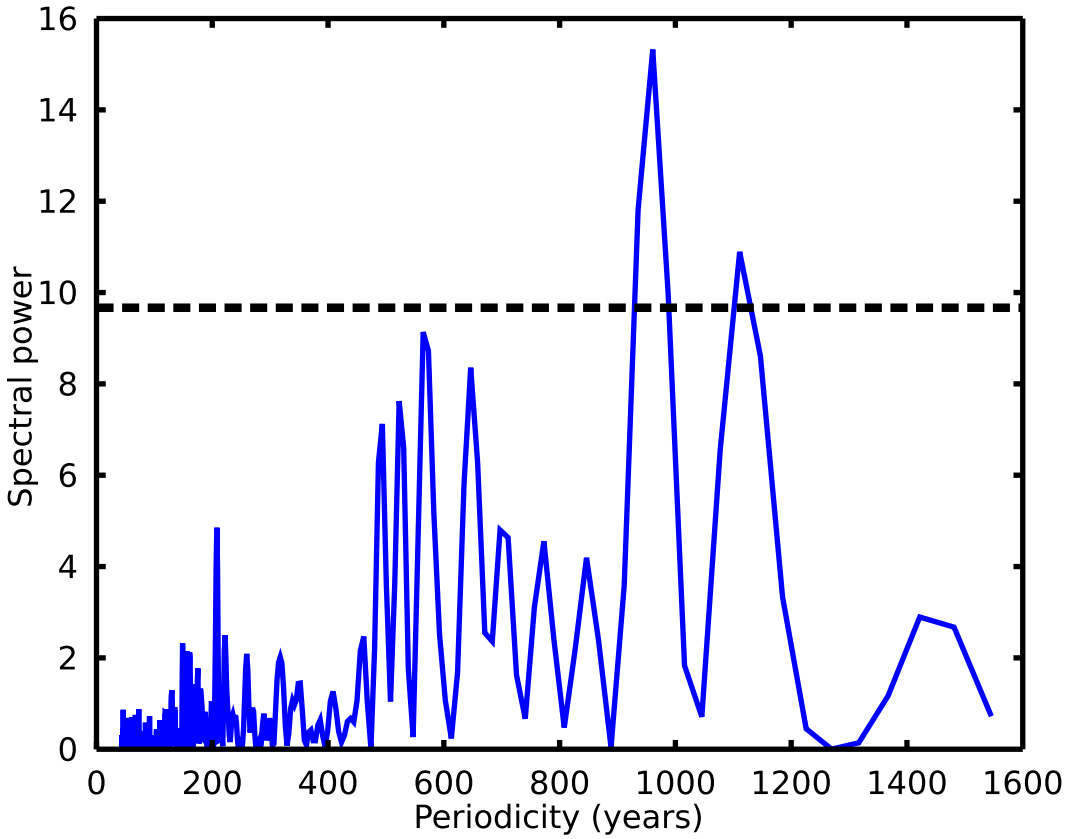

Figure S17 Lomb normalized periodogram (spectral power as a function of periodicity) of the Asian climate record ($\delta^{18}O$) from Dongge cave, China, (29). The horizontal line marks the 95% significance level. Prominent periodicities of solar activity (de Vries cycle at ~210 years and the Eddy cycle at ~1000 years (28)) are found in the climate record (see Figure S16 for periodogram of solar activity). The de Vries cycle is not significant at the 95% level.

S12. Correlation analysis

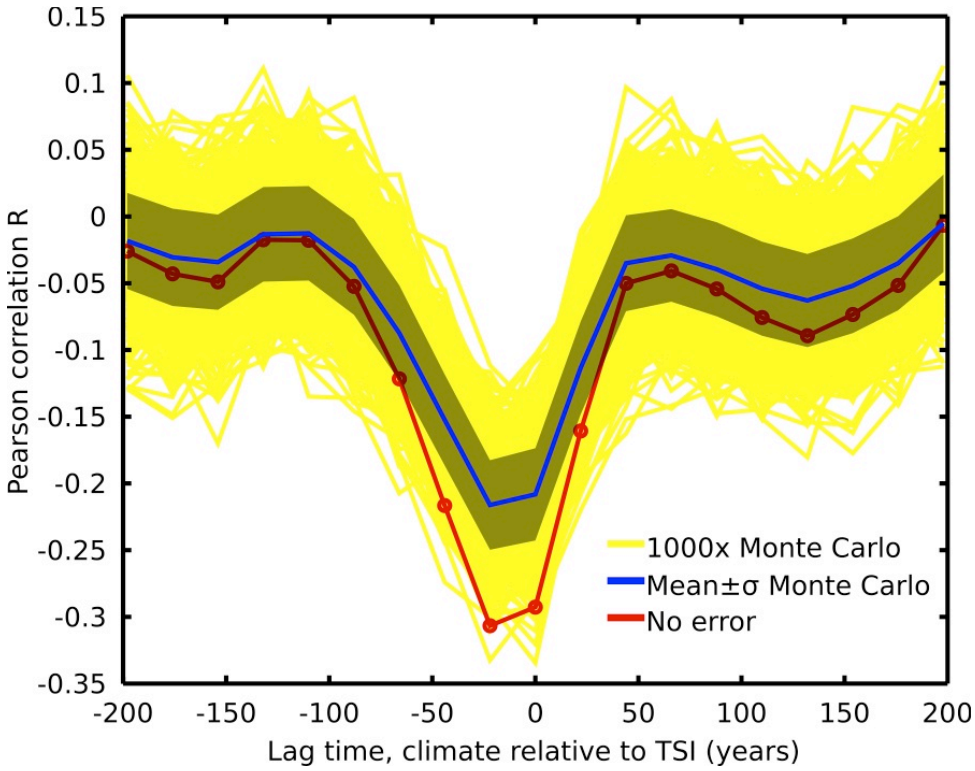

Figure S18 Pearson correlation as a function of lag time between the $\delta^{18}O$ record of Asian monsoon (29) and total solar irradiance (TSI). Both time series are 22-year averages, linearly detrended and high-pass filtered with 2000 years. Lag time is climate time relative to TSI time, i.e. a lag time of 100 years means the climate record lags TSI by 100 years. To consider the uncertainty in the records, we performed 1000 Monte Carlo simulations. For reasons of simplicity we assumed that the time scales in both records and the $\delta^{18}O$ signal have no uncertainty. All uncertainty was put into the TSI signal ($\Delta TSI=1Wm^{-2}$). The yellow curves in the background show the individual lag correlation curves from the Monte Carlo simulations. The blue curve is the mean value and the standard deviation from the Monte Carlo simulations at individual lag times. The red curve is the result without consideration of any uncertainty (strongest correlation is R=0.31 at the lag time -22 years, the correlation with no lag is R=0.29). The strongest correlation is found for a slightly negative lag time, which is consistent with no lag within the Monte Carlo uncertainty.

S13. Comparison of total solar irradiance (TSI) with published reconstructions

In figures S19 and S20 the time series of total solar irradiance of this study is compared with two existing reconstructions also covering the Holocene. The reconstructions are abbreviated with SEA09 (19) and.with VEA11 (30). SEA09 is based on the ^{10}Be record from GRIP ice core and VEA11 is based on the ^{14}C INTCAL04 record. Both records are used in this paper. In this paper the GRIP time scale is GICC05 whereas the GRIP timescale ss09 is used in SEA09, and that in this paper the updated ^{14}C INTCAL09 record is used instead of INTCAL04 that is used by VEA11. As can be seen from the panels a and b in both figures there is a good agreement between the curves except that the amplitudes of individual grand solar minima are different. The difference between TSI of this study and SEA09/VEA11 (panel b in both figures) show short-term variability but no long-term trend. The panels c in the figures show the wavelet coherence. At short periodicities the coherence has very little power whereas the coherence is high at longer periodicities. This can be explained by the fact that system effects occur mainly on shorter time scales (<100 years). Thus, the wavelet coherence panels clearly point to a noise reduction in the derived TSI record of this study compared to the former records SEA09 and VEA11 which are based on individual radionuclide

records only.

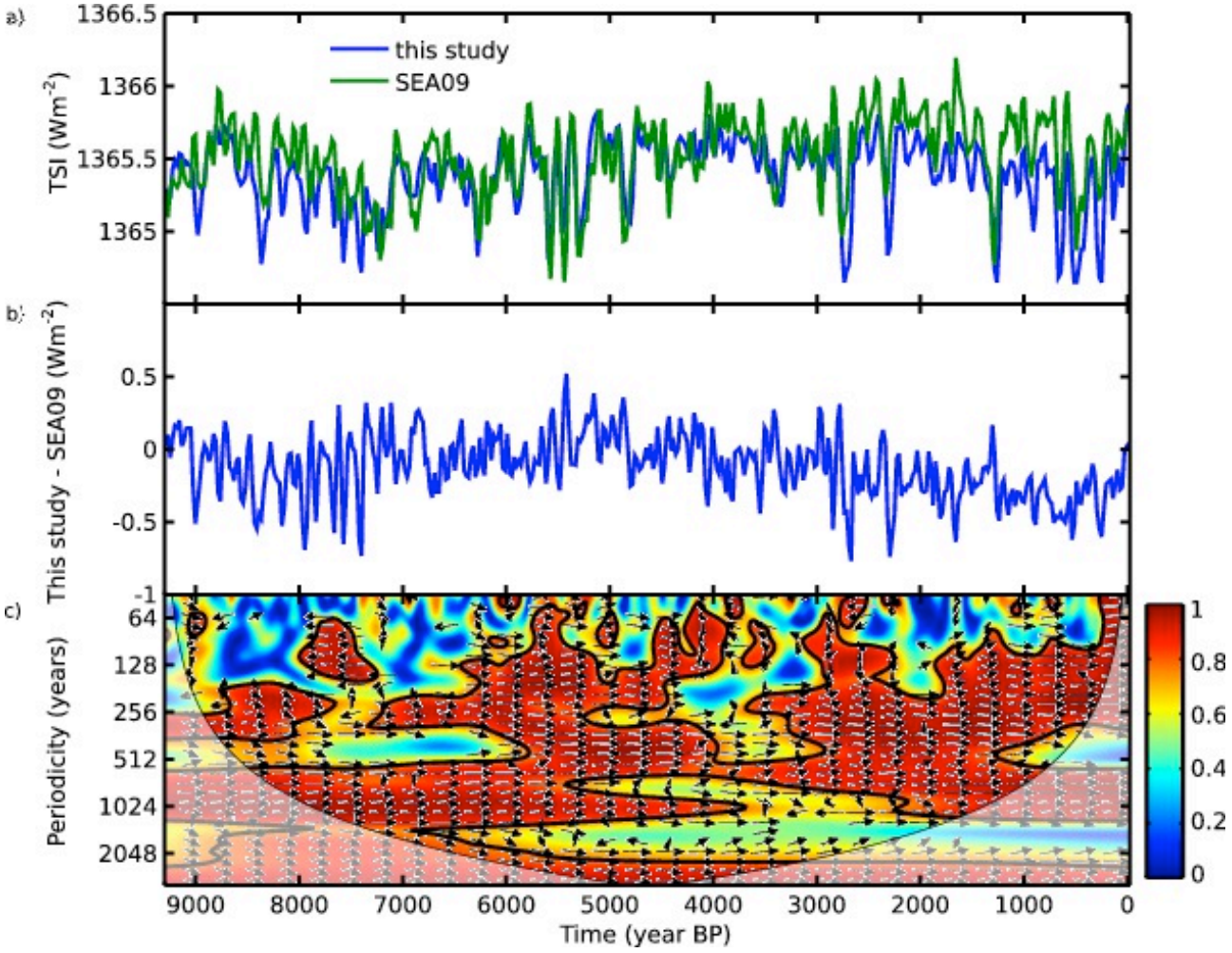

Figure S19 Comparison of TSI of this study with SEA09 (19). Time is given in year BP. a) Time series of TSI of this study (blue) and SEA09 (green). SEA09 was averaged to 22 years to be comparable with TSI of this study. b) Difference. c) Wavelet coherence. Arrows pointing to the right are in phase. Black boundaries mark regions with 95% significance.

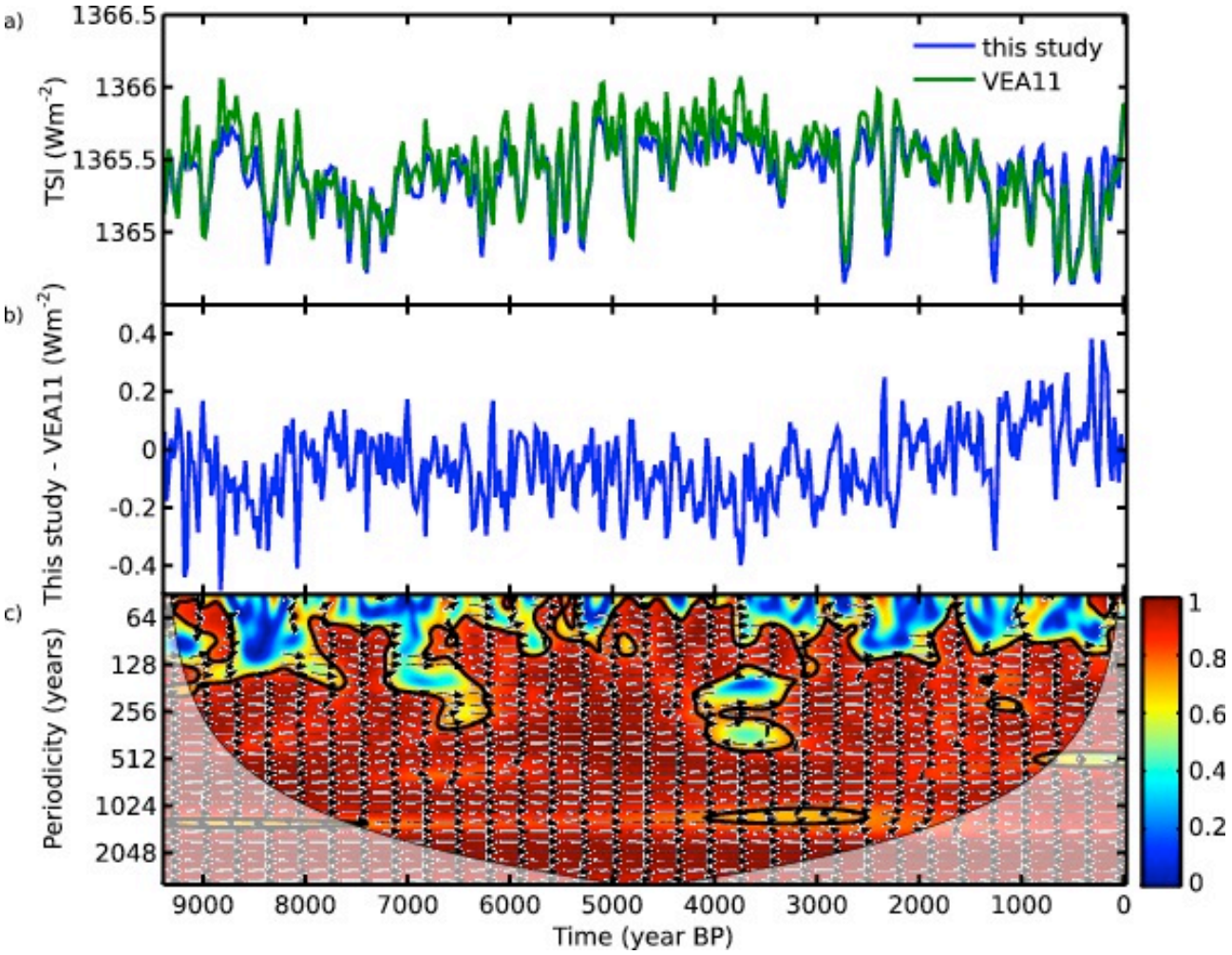

Figure S20 Comparison of TSI of this study with VEA11 (30). Time is given in year BP. a) Time series of TSI of this study (blue) and VEA11 (green). VEA11 are originally 10-year averages and was averaged to 22 years to be comparable with TSI of this study. b) Difference. c) Wavelet coherence. Arrows pointing to the right indicate that the data are in phase. Black boundaries mark regions with 95% significance.

References

1. *Masarik J & Beer J (2009) An updated simulation of particle fluxes and cosmogenic nuclide production in the Earth's atmosphere. J Geophys Res-Atmos 114:D11103.*
2. *Reimer PJ, et al. (2009) Intcal09 and Marine09 Radiocarbon Age Calibration Curves, 0-50,000 Years Cal Bp. Radiocarbon 51(4):1111-1150.*
3. *Yiou F, et al. (1997) Beryllium 10 in the Greenland Ice Core Project ice core at Summit, Greenland. J Geophys Res-Oceans 102(C12):26783-26794.*
4. *Muscheler R, et al. (2004) Changes in the carbon cycle during the last deglaciation as indicated by the comparison of Be-10 and C-14 records. Earth Planet Sc Lett 219(3-4):325-340.*
5. *Beer J, Tobias S, & Weiss N (1998) An active sun throughout the Maunder Minimum. Sol Phys 181(1):237-249.*
6. *Beer J, et al. (1985) Accelerator Measurements of Be-10 - the 11 Year Solar-Cycle from 1180-1800 Ad. Nucl Instrum Meth B 10-1(MAY):415-418.*
7. *Berggren AM, et al. (2009) A 600-year annual Be-10 record from the NGRIP ice core,*

Greenland. Geophys Res Lett 36:L11801.

8. *Raisbeck GM, Yiou F, Jouzel J, & Petit JR (1990) Be-10 and Delta-H-2 in Polar Ice Cores as a Probe of the Solar Variability Influence on Climate. Philos T Roy Soc A 330(1615):463-470.*
9. *Horiuchi K, et al. (2008) Ice core record of Be-10 over the past millennium from Dome Fuji, Antarctica: A new proxy record of past solar activity and a powerful tool for stratigraphic dating. Quat Geochronol 3(3):253-261.*
10. *Epica Community Members (2006) One-to-one coupling of glacial climate variability in Greenland and Antarctica. Nature 444(7116):195-198.*
11. *Kubik PW & Christl M (2010) Be-10 and Al-26 measurements at the Zurich 6 MV Tandem AMS facility. Nucl Instrum Meth B 268(7-8):880-883.*
12. *Ruth U, et al. (2007) "EDML1": a chronology for the EPICA deep ice core from Dronning Maud Land, Antarctica, over the last 150 000 years. Clim Past 3(3):475-484.*
13. *Korschinek G, et al. (2010) A new value for the half-life of Be-10 by Heavy-Ion Elastic Recoil Detection and liquid scintillation counting. Nucl Instrum Meth B 268(2):187-191.*
14. *Chmeleff J, von Blanckenburg F, Kossert K, & Jakob D (2010) Determination of the Be-10 half-life by multicollector ICP-MS and liquid scintillation counting. Nucl Instrum Meth B 268(2):192-199.*
15. *Siegenthaler U (1983) Uptake of Excess CO_2 by an Outcrop-Diffusion Model of the Ocean. J Geophys Res-Oc Atm 88(NC6):3599-3608.*
16. *Usoskin IG, Bazilevskaya GA, & Kovaltsov GA (2011) Solar modulation parameter for cosmic rays since 1936 reconstructed from ground-based neutron monitors and ionization chambers. J Geophys Res-Space 116:A02104.*
17. *Steinhilber F, Abreu J, & Beer J (2008) Solar modulation during the Holocene. Astrophysics and Space Sciences Transactions 4(1):1-6.*
18. *Steinhilber F, Abreu JA, Beer J, & McCracken KG (2010) Interplanetary magnetic field during the past 9300 years inferred from cosmogenic radionuclides. J Geophys Res-Space 115:A01104.*
19. *Steinhilber F, Beer J, & Frohlich C (2009) Total solar irradiance during the Holocene. Geophys Res Lett 36:L19704.*
20. *Vonmoos M, Beer J, & Muscheler R (2006) Large variations in Holocene solar activity: Constraints from Be-10 in the Greenland Ice Core Project ice core. J Geophys Res-Space 111(A10):A10105.*
21. *Gleeson LJ & Axford WI (1968) Solar Modulation of Galactic Cosmic Rays. Astrophys J 154(3P1):1011-1026.*
22. *Knudsen MF, et al. (2008) Variations in the geomagnetic dipole moment during the Holocene and the past 50 kyr. Earth Planet Sc Lett 272(1-2):319-329.*
23. *Herbst K, et al. (2010) On the importance of the local interstellar spectrum for the solar modulation parameter. J Geophys Res-Atmos 115:-.*
24. *Garciamunoz M, Mason GM, & Simpson JA (1975) Anomalous He-4 Component in Cosmic-Ray Spectrum at Less Than Equal to 50 Mev Per Nucleon during 1972-1974. (Translated from English) Astrophys J 202(1):265-275 (in English).*
25. *Korte M & Constable CG (2005) The geomagnetic dipole moment over the last 7000 years - new results from a global model. Earth Planet Sc Lett 236(1-2):348-358.*

26. *Rouillard AP, Lockwood M, & Finch I (2007) Centennial changes in the solar wind speed and in the open solar flux. (Translated from English) J Geophys Res-Space 112(A5):- (in English).*

27. *Frohlich C (2009) Evidence of a long-term trend in total solar irradiance. Astron Astrophys 501(3):L27-U508.*

28. *Abreu JA, Beer J, & Ferriz-Mas A (2010) Past and future solar activity from cosmogenic radionuclides. Astronomical society of the pacific conference series: SOHO-23: Understanding a peculiar solar minimum, Editors: S.R. Cranmer, J.T. Hoeksema, J.L. Kohl 428.*

29. *Wang YJ, et al. (2005) The Holocene Asian monsoon: Links to solar changes and North Atlantic climate. Science 308(5723):854-857.*

30. *Vieira LEA, Solanki SK, Krivova N, & Usoskin I (2011) Evolution of the solar irradiance during the Holocene Astron Astrophys.*